Conformational state switching and pathways of chromosome dynamics in cell cycle

Xiakun Chu, and Jin Wang*

Department of Chemistry
State University of New York at Stony Brook, Stony Brook, NY 11794, USA

* jin.wang.1@stonybrook.edu

October 8, 2019

Significance Statement

Cell cycle progression is intimately related to the chromosome dynamics. A quantitative and physical description of chromosome structural transition between de-condensation at interphase and condensation at mitotic phase is still missing. We developed an excitation-relaxation energy landscape-switching model along with the maximum entropy principle to investigate the cell cycle-dependent chromosome dynamics. The stochastic yet non-random chromosome conformational transition pathways were uncovered. They are irreversible due to the detailed balance breaking of the underlying non-equilibrium dynamics. In addition to the good agreement with the experimentally suggested mitotic chromosome folding process, we made extensive predictions that can be assessed in the future experiments. Our findings and approach can be applied to other biological processes far from equilibrium.

1 Abstract

Cell cycle is vital for cell function. During the cell cycle, chromosome structurally alternates between condensation and de-condensation states in favor of biologically distinct functions at mitotic (M) phase and interphase (I phase). However, it is still unclear how chromosome dynamically operates such large-scale conformational changes between different phases during the cell cycle. We aim to resolve this issue by developing an excitation-relaxation energy landscape-switching model combining with the maximum entropy principle. Our approach includes non-equilibrium effects explicitly, thus can capture the essence of the cell-cycle dynamics far from equilibrium. We quantitatively identified the chromosome conformational transition pathways between the I and M phases in both directions and found they are irreversible and highly heterogeneous, though not random. Heterogeneity reflects the cell-to-cell variability of the cell-cycle dynamics, in line with the single-cell Hi-C experiments. Our results are in good agreement with the experimentally suggested two-stage chromosome condensation process, where interphase chromosome linearly compacts into consecutive loops, followed by the axial compression. The irreversible pathways are due to distinct interplays between short- and long-distance interactions in the two directional chromosome transformations. We further attribute the irreversibility of chromosome conformational transition during the cell cycle to the non-equilibrium dynamics driven by the energy excitation from the underlying chemical reactions. We draw a complete dynamic picture of chromosome structural transformation during the cell cycle. Our findings provide crucial insights into the relationships among the spatial organization, conformational dynamics and biological function of chromosome.

2 Introduction

There is little doubt that the fundamental structure-function paradigm in biology preserves in a broad range from the very simple single molecule unit such as protein to the highly complex biopolymer assembly such as genome [1]. The biologically functional 3D genome organization has been known to facilitate the gene regulation in terms of engaging two distal enhancer and promoter in physical proximity [2]. However, the details of the connections between structure and function at genomic level are far from clear, as quantifying the spatial organization of genome has been a long-time challenging issue for biologists. Based on the use of DNA-DNA ligation assays, Chromosome Conformation Capture (3C) [3] and its derivative Hi-C method [4] have been rapidly developed since the last two decades. The techniques count the frequency of genomic loci spatially close to each other, therefore are highly informative to infer the structure arrangement of genome. Recent studies have harnessed the power of Hi-C and comprehensively investigated the chromosome structural changes during the cell cycle [5, 6, 7, 8, 9], where the chromosome exhibits functionally important dynamics between cyclic condensation and de-condensation. Such studies at Hi-C resolution have profoundly enhanced our understanding of the structure-function relationship at the genomic level.

Carefully examining the interphase Hi-C data has uncovered two major structural characteristics for chromatins at different levels: topological associated domains (TADs) [10, 11, 12, 13] and compartments [4]. TADs are characterized by more frequently formed contacts within such megabase-sized domains

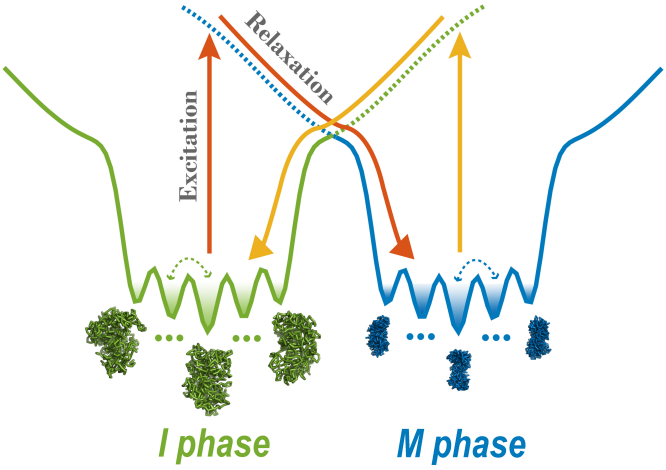

Fig. 1: A scheme illustrating the energy landscape-switching model for simulating the chromosome transformation during the cell cycle. There are two energy landscapes, each with one prominent basin, representing chromosome at the I and M phase respectively. Within each basin, there are many potential energy minima, corresponding to different metastable chromosome states. Simulation starts from one structure at the I phase (or M phase) basin and runs for a period of times. Then a sudden excitation action by switching of the energy landscape to the M phase (or I phase) is implemented. Finally, the system relaxes to the new basin within the post-switched energy landscape. We found that the transition between the sub-minima within one basin (phase) is a very slow process and can not be faithfully achieved (Fig. S5 and S9). The extremely low rate to full equilibration along with the highly heterogeneous subdiffusivity of individual chromosomal locus manifests that the chromosome conformational dynamics within either the I or M phase is glassy-like [20].

than that with the outside neighboring regions, while compartments segregate the chromatin in terms of the plaid contact patterns at long-range scale (usually $\sim$ 5 Mb). TADs have been hypothesized as the fundamental units [14] not only for the chromosome folding [15], but also for genome function at interphase, including the modulations of DNA replication [16] and regulation at the transcription level [17]. Recent Hi-C datasets of the cell cycle clearly show that TADs and compartments in interphase vanish during mitosis [7, 9]. Furthermore, Hi-C characterized a significant global reshaping of the chromosome from a crumpled fractal globule at the interphase [18] to a condensed quiescent cylinder at the metaphase. Such highly condensed cell-type independent mitotic chromosome favors the movement and separation of genome during cytokinesis, but potentially represses the transcription by limiting the accessibility of promoter regions to the transcription factors [19]. These features underline the prevalence of chromosome structure-function regulation that acts distinctly at different cell cycle stages.

3C experiments only draws a static portrait of spatial chromosome organization, while chromosome dynamics is closely related to the activation of transcriptions and gene regulations [21, 22]. At the long time scale, chromosomal loci exhibit collective movements [23], which can still be active even beyond the boundary of the TADs and chromosomal territories. This observation indicates that the dynamics among the chromosomal locus is somehow coupled mechanically rather than structurally. It is seemingly deviated from the protein experience that the structures inherently guide the dynamics. Such unprecedented complexities require the improvements of current research approach on the chromosomes by considering both the structure and dynamics, simultaneously.

Up to now, a quantitative and physical picture of dynamic chromosome structural change during cell division is still missing. Such picture pursued as a key question in cell biology, would ultimately clarify the distinct roles of the structural maintenance of chromosome (SMC) protein complexes in organization of chromosome during the cell cycle [24, 25]. Practically, a combination of Hi-C data and theoretical modelling seems to be ideal. However, challenges come in three ways: faithful development of theoretical models that can reproduce the Hi-C data, efficient performance of the simulations that can capture the day-long cell cycle process and the applicability of simulations for non-equilibrium cell-cycle dynamics. Here, we resolved the above-mentioned issues by developing an excitation-relaxation energy landscape switching model along with the maximum entropy principle.

Chromosome dynamics within either the I or M phase may be constantly under the influence of the non-equilibrium effects from the surrounding cellular environments. Nevertheless, it has been demonstrated that the effective equilibrium landscape is capable to describe the non-equilibrium dynamics in some circumstances [26, 27]. The minimally biased energy landscapes led by maximum entropy principle for chromosome dynamics have been practically proved successful in quantifying the spatial organizations of interphase [28] and mitotic chromosome [29] from sparse Hi-C data. Based on the previous investigations by us [30, 31, 32] and many others [33, 34], it seems to be intuitive to develop a "two-basin" energy landscape that inherits from each individual phase-dependent landscape with reasonable connections in between [33] to investigate the chromosome dynamics during the phase-to-phase transition. However, as an extremely long polymer chain in a strongly confined space, chromosome in cell exhibits glassy behavior [35], indicating that chromosome may never fully equilibrate even within one phase. More importantly, it is unreasonable to construct the equilibrium "two-basin" energy landscape for the cell-cycle dynamics, which is an active process far from the thermodynamic equilibrium and sensitive under the control of complex regulatory network [36]. This poses a great challenge on exploring the cell-cycle chromosome dynamics via simulations.

The cell-cycle dependent chromosome transformation is biologically participated by various SMC proteins and other biochemical agents [37]. From the physical viewpoint, the process is driven by the forces originated from the non-equilibrium dynamics led by chemical reactions through ATP hydrolysis. We have demonstrated that the cell-cycle dynamics is determined by both the potential landscape and curl probability flux [38, 39]. While the landscape stabilizes the states along the cell cycle, the non-zero flux, which reflects the degree of the detailed balance breaking or nonequilibriumness [40], drives the stable cell cycle oscillations. Therefore, the effects of the metabolic energy supplies for driving the cell cycle should be

taken into account for simulating the processes with efficiency and validity. Here, we mimic such non-equilibrium effect by an "energy excitation" process that ensures the chromosome to successfully transform from one effective energy landscape to the other. In practice, it is implemented by a sudden switch of the chromosome energy landscape from the I (M) phase to M (I) phase (Fig. 1). Such switching implementation has clear biological correspondence, where chromosome gains the energy after cell is regulated to trigger the cycle progression by the rapid change of cyclin concentration [41]. Furthermore, the energy landscape-switching implementation leads to a non-equilibrium cell-cycle dynamics in accordance with the process occurring in the cells. The broken detailed balance caused by non-equilibrium dynamics is expected to have unprecedented effects on chromosome conformational transitions [40], in contrast to the conventional equilibrium dynamics. The rational of our models for simulating the cell cycle process is based on the assumption that the slow conformational dynamics of chromosome is driven by the external stimuli (i.e. energy pump from ATP hydrolysis). This is seemingly reasonable, as the entire extremely long chromosome never fully equilibrates in the cell cycle time [42] and the local TADs also fluctuate on the time scales of minutes [43].

We have identified statistically sufficient number of cell-cycle dynamics-dependent chromosome pathways, which are highly heterogeneous, though not random. We uncovered the irreversibility in the ensemble-averaged chromosome transition pathways of the two directional transitions between the I and M phases. This reflects the utilization of metabolic energy supplied by different SMC or other biochemical agents during different cell cycle stages [44]. The pathways also show a two-stage mitotic chromosome folding, and exhibit faster conformational contact formation at local rather than long distance. Our results are in good agreement with the existing experimental findings [45, 7, 9] and lead to extensive predictions. The picture we drew here provides quantitative explanations to further decipher the dynamic regulation of structure-function relationship in chromosome during the cell-cycle dynamics.

3 Results

3.1 Cell cycle chromosome conformational dynamics triggered by energy landscape-switching

We used a generic polymer model simulations that were constantly restrained by Hi-C data through the maximum entropy principle to explore the chromosome dynamics in the I phase and M phase separately. The models have successfully reproduced the experimental Hi-C data characteristics, such as segregated hierarchical compartmentalization and TADs leading to crumpled fractal globular chromosome at the I phase (Fig. S2 and S3), as well as the elimination of compartments and TADs in condensed cylindrical chromosome at the M phase (Fig. S6 and S7). These facts demonstrate the validity of our approach in modelling the chromosome structures from the sparse Hi-C data. Going beyond the thermodynamic structural distributions, we investigated the spatiotemporal chromosome dynamics at the I phase by calculating the mean square displacement (MSD) and compared to the available experimental measurements [46]. The sub-diffusive behavior, which has been observed in the experiments, was successfully predicted by our model (Fig. S5). Quantitatively, the diffusion scaling factor $\beta = 0.45$ in MSD $\sim t^{\beta}$ at interphase matches very well with that measured in experiments [46]. Therefore, the potential generated by the maximum entropy principle, referring to as an effective energy landscape, can be used to realistically reproduce the correct thermodynamic distribution of chromosome conformation and kinetic diffusivity of individual locus simultaneously, providing the basis for our following modelling and simulations.

The energy landscape-switching approach allows us to observe the chromosome conformational transition between the I and M phase during the cell cycle. As shown in Fig. 2, the circle at the center exhibits apparent cyclic change of contact probability P_s on varying genomic distance s during the cell cycle. P_s characterizes the conformational transformation quantitatively between the fast decrease s^{-1} at the I phase and slow decrease $s^{-0.5}$ at the M phase (Fig. S12). Notably, P_s shows dramatic changes even at the beginning of the relaxation time period in both of the two directional transitions, indicating a fast response at chromosome conformation to the landscape-switching. Bearing in mind that chromosomes often appear to be trapped in multiple disconnected metastable states for remarkably long time on the effective energy landscape within either the I or M phase [47] (Fig. S5 and S9), here we clearly showed that the cell-cycle dynamics has been efficiently activated and successfully achieved by the energy landscape-switching.

Evolution of the contact probability heat maps clearly show that chromosome transformation proceeds with condensation (de-condensation), loss (formation) of TADs and compartments in the transition of I $\rightarrow$ M (M $\rightarrow$ I) (Fig. 2). In transition from the I to M phase, chromosomes initially exhibit the characteristics in the I phase at $t = 0\tau$. After a very short time lag at $t = 1\tau$, there are observably widespread changes on contacts, leading to the slight deviations of TAD and compartment profiles from those in the I phase. Such rapid and acute response reflected by chromosome organization to the phase switching has also been found in the experimental Hi-C when G_2 cells enter into the prophase [9]. Further cell cycle progression continuously increases the condensation extents of the chromosome along with the gradual loss of TADs and compartments. At $t = 100\tau$, TADs seem to be completely lost consistent with what appears in the M phase, while notable extents of compartment still possess at certain regions. Completely disappearance of the compartment profile in chromosome can emerge beyond $t = 1000\tau$ (Fig. S13). These features indicate that short-distance chromosome conformations form faster than long-distance ones during I $\rightarrow$ M transition.

On the other hand, a sharp loss of contact formation can be observed at the very beginning of M $\rightarrow$ I transition at $t = 0.1\tau$ (Fig. S14). However, this does not make apparent contribution to compartment or TAD formation (Fig. S13). At $t = 1\tau$, TAD starts to be strengthened and compartments appears to be deviated from that in the M phase. Both of the TADs and compartments are almost formed during the time from $t = 1\tau$ to $t = 100\tau$ (Fig. 2). It is worth noting that there can be more contacts lost at $t = 1\tau$ than the final destined I phase (Fig. S14).

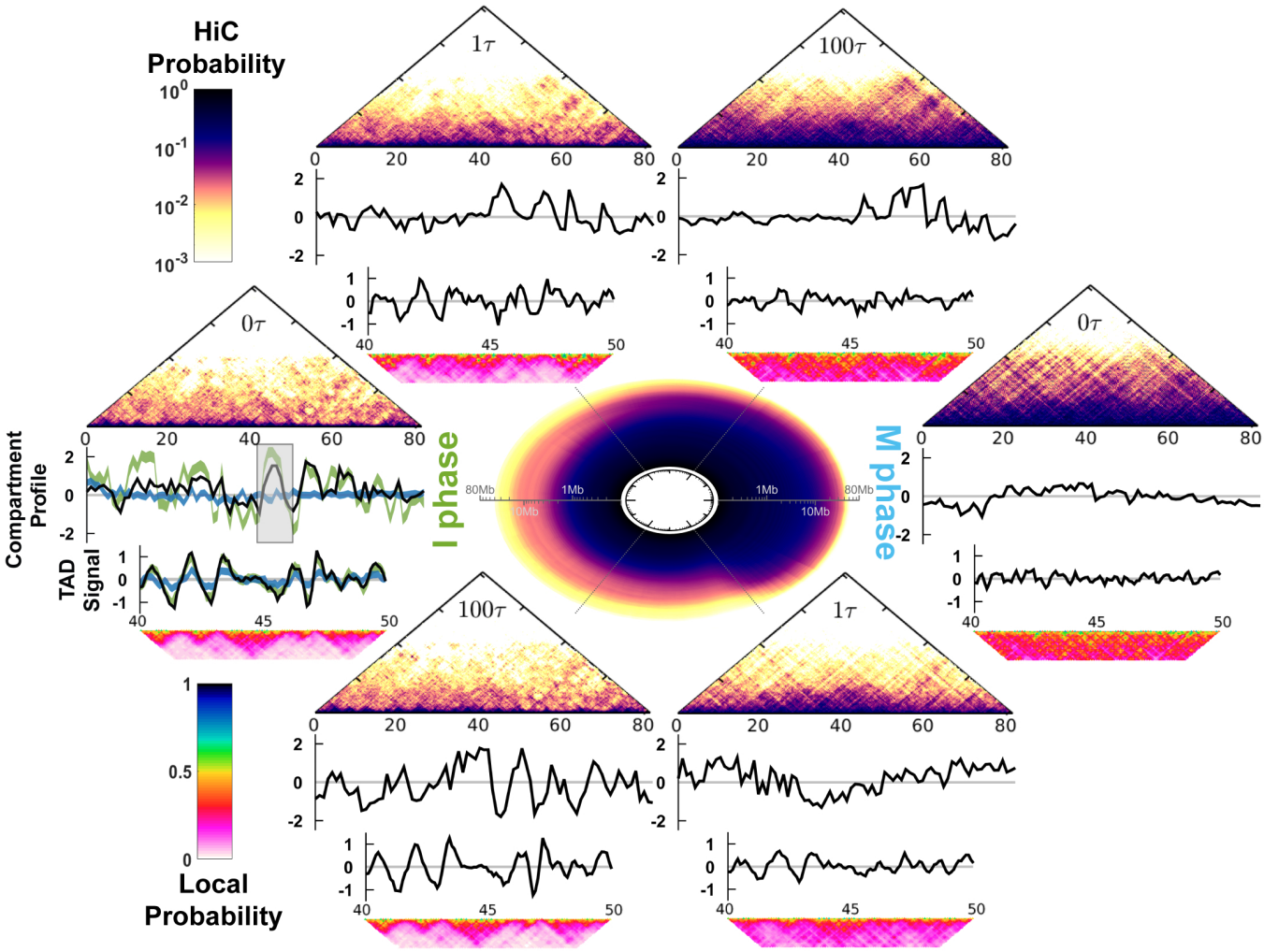

Fig. 2: Chromosome transformation during the cell cycle. The circle at the centre represents the contact probability $P_s(t)$ along the genomic distance s evolving during the cell cycle that goes clockwise. The radial and angular coordinate of the circle are respectively the genomic distance s and cell cycle processing time t with both shown in logarithmic scale. The up semicircle describes the transition from the I to M phase, while the down semicircle describes the transition from the M to I phase. At particular time points $t = 0\tau$, 1τ, 10τ and 100τ the corresponding Hi-C-like contact map, compartment profile, TAD signal and short-distance contact map at 40-50 Mb regions are shown. In the leftmost panel, the transparent green and blue lines at the compartment profile and TAD signal plots are the values calculated from Hi-C data for the I and M phase, respectively.

This implies that chromosome may possess an over-expansion configuration around $t = 1\tau$. From $t = 1\tau$ to $t = 100\tau$, a delicately compartmentalized conformational quenching at long-distance and formation of TAD are expected. These features imply that the formation of short- and long-distance chromosome conformations is almost synchronous during the transition from the M to I phase. Overall, we show that chromosome undergoes cycle of condensation and de-condensation, proceeding along with the cell cycle stages. However, the compaction and expansion processes in I-to-M and M-to-I phase transitions may not follow the same routes.

3.2 Cell cycle chromosome conformational evolution

We then collected all the simulated trajectories during the phase transitions and projected them to certain order parameters to quantify the transition pathways between the I and M phase (Fig. 3 and 4). We firstly focused on the global structural change of chromosome by examining the extension lengths along the principle axes (PA) [29], aspheric shape parameter (Δ) [48] and radius of gyration (R_g). PA and Δ are determined from the eigenvectors and eigenvalues of the inertia tensor (Details in SI). The deviation of Δ from 0 quantifies the extent of the anisotropy [48]. The distributions of the three PA extensions and Δ of chromosome show a more spherical polymer chain at the I phase in contrast with that of the M phase with a cylindrical shape (Fig. S3 and S7). The results are consistent with previous polymer models and simulations [4, 29, 45].

Once the energy landscape-switching is triggered from the I to M phase, chromosome starts compaction by decreasing both of the extension lengths at the PA1 and PA3, which are defined as the longest and shortest extensions respectively (Fig. 3A). The apparent individual pathways are highly heterogeneous and there is no dominant path that can be defined. Nevertheless, all the pathways exhibit stochasticity following par-

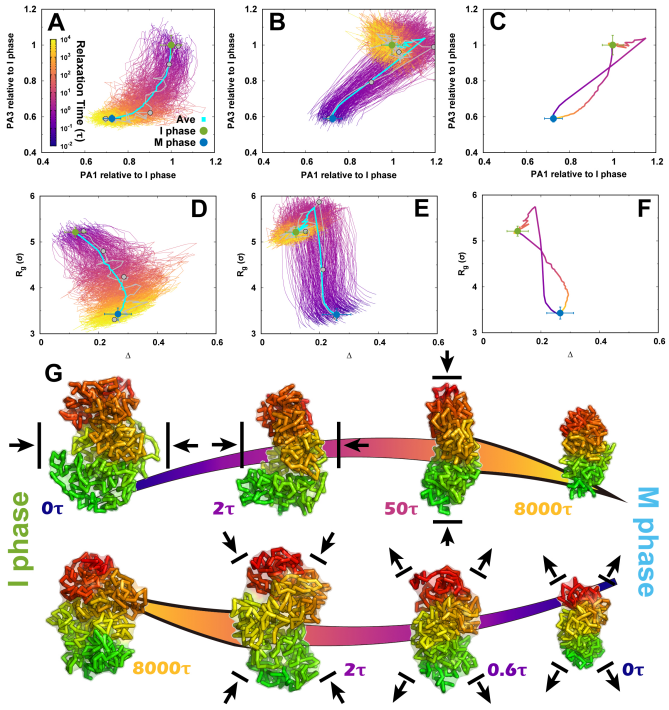

Fig. 3: Shape evolution of chromosome conformation during the cell cycle. (A) The pathways projected onto the extension lengths along the first and third principal axes (PA) during the transition from the I to M phase. The first and third PA are defined to have the longest and shortest extensions of the chain conformation, respectively. Relative PA extension lengths to the mean values of those in the I phase are used. Thus the transition approximately starts from (1, 1) and decreases in condensation process to the M phase. All the transition trajectories are shown and colored by time in logarithmic scale. The mean values in the I and M phase are present with green and blue points. The pathway averaged by all trajectories is shown with the cyan line. (B) Same with (A) but for the transition from the M to I phase. (C) The average pathways colored by logarithmic timescale for the two directional transitions. (D) The pathways projected onto the aspherical parameter Δ and radius of gyration R_g during the transition from the I to M phase. Δ is in the range of 0$\sim$1. For perfect spheres, $\Delta = 0$. (E) Same with (D) but for the transition from the M to I phase. (F) The average pathways for the two directional transitions. (G) Typical structures extracted from the transition trajectories with top ones corresponding to I $\rightarrow$ M transition and bottom ones corresponding to M $\rightarrow$ I transition. The selected pathways are shown in (A), (B) and (D), (E) by grey lines with points corresponding to the positions of the representative structures. Chromosome structures are colored from red to green scheme varied by the genomic distance. The black arrows along with the structures illustrate the major shape changes expecting for the next evolution step.

ticular rules to accomplish the condensation process. We can readily see that most of the chromosomes likely adopt to compact more at the PA3 than PA1 dimensions at early stage, while shortening the extension of PA1 is more significant in majority at late stage. It can also be reflected by the averaged pathway. Further projecting the pathways onto R_g and Δ provides a consistent and complementary explanation for the transition (Fig. 3D). At the beginning, R_g and Δ decrease and increase respectively at a nearly synchronous step, resulting in an anisotropic compaction of chromosome conformation, while continuously decrease of R_g along with unchanged and even slightly decrease of Δ are found at late stage. The late step is in accordance with the picture that chromosome shortens the extension at longest PA to eventually form the mature mitotic conformation. The typical structures extracted from one particular trajectory which is close to the average pathway clearly show how chromosome evolves to condensed cylinder (Fig. 3G). The picture is highly in line with the two-stage mitotic chromosome folding hypothesis, where interphase chromosome linearly compacts into consecutive loops, followed by the axial compression [45].

The transition of M $\rightarrow$ I, interestingly, provides a different picture of chromosome de-condensation, which is not a simple reversal of chromsome condensation in the transition of I $\rightarrow$ M. As shown by the trajectories of the extension lengths of PA, chromosomes utilize rapid isotropic expansions at early stage, and then preferentially reach a distinct set of configurations that have even larger extensions along PA1 dimension than chromosome at the I phase (Fig. 3B). Such observation can also be readily seen by looking at the pathways projected onto R_g and Δ (Fig. 3E), where a rapid increase on R_g at early stage till a bigger R_g beyond the one at the I phase is achieved during the transition (Fig. 3E). This indicates that chromosome over-expands its conformation primarily along its longest axes dimension. Quenching from the over-expanded chromosome conformation to that in the I phase requires extraordinary compaction along PA1, resulting in a slight condensation process to the globule-like shape shown in terms of decreasing R_g and Δ simultaneously.

Finally, the average pathways for the two directional transitions show completely different routes connecting the I and M phase (Fig. 3C and 3F), leading to the conclusion that the cell-cycle dynamics of chromosome transformation is stochastic and irreversible.

We then used the quantities related to contact formation to project the pathways (Fig. 4). The contact order parameters include the fraction of contacts Q, which is similar with that widely used in protein folding, but with the reference to chromosome ensemble average in either the I or M phase rather than one single existing structure, and the Hi-C-like contact probability P. The subscriptions of Q and P represent the genomic distance range of contacts formed by pairwise beads. It is worth noting that at both the I and M phases, Q presents relatively low values compared to that in protein folding and the local Q is higher than non-local Q. It implies that there are remarkable fluctuations to the ensemble average with more diverse non-local than local chromosome conformations in both the I and M phase [28].

In transition of I $\rightarrow$ M, the similarity of the local chromosome conformation to I and M phase decreases and increases simultaneously at the initial stage (Fig. 4A). Then after Q^M_{0-2Mb} reaches a plateau (>0.5), which is even a little higher than the value in the final M phase, breaking the local conformation formed in the I phase becomes dominant in finalization of the transition. On the other hand, the non-local contacts initially proceed to form the destined conformation

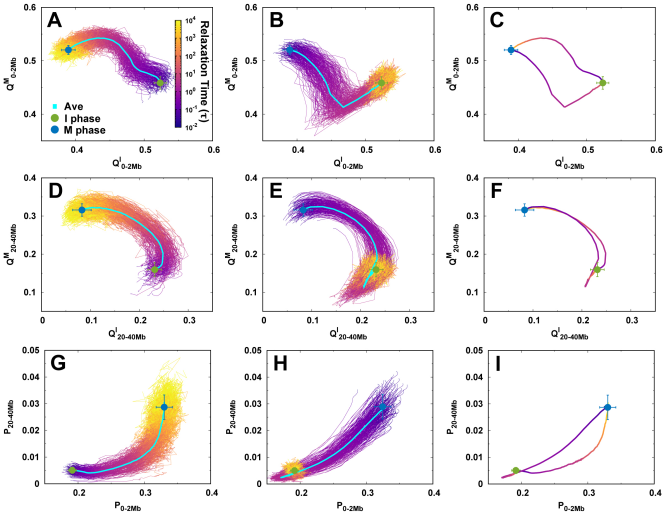

Fig. 4: Contact structural evolution of chromosome conformation during the cell cycle. (A-C) The pathways projected onto the local conformational order parameters. $Q^{I(M)}_{0-2Mb}$ is the fraction of contacts formed by the pairwise loci that are in the genomic distance from 0 to 2 Mb, with superscript I and M respectively corresponding to the references chosen from the I and M phase. The references are the average pairwise distances in the I or M phase ensemble (Fig. S3 and S7). Pathways for (A) I $\rightarrow$ M transition, (B) M $\rightarrow$ I transition, as well as (C) the average for the two directional transitions are present. (D-F) and (G-I) are the same with (A-C) but respectively projected onto the non-local conformational order parameter $Q^{I(M)}_{20-40Mb}$ and contact probability P at short (0-2Mb) and long (20-40Mb) distances.

in the M phase without disturbing that in the I phase; then a nearly synchronous step in decreasing $Q^{I}_{20-40Mb}$ and increasing $Q^{M}_{20-40Mb}$ can be seen; finally the last step to the M phase mainly corresponds to the breaking the formation of contacts that are in the I phase (Fig. 4D). The picture shows the local and non-local chromosome conformation undergo asynchronous step in transition, as can be readily observed by retrieving the pathways projected onto the local and non-local contact probability (Fig. 4G). Local contacts tend to form prior to non-local contacts in transition from the I to M phase.

Intriguingly, the local contact formation proceeds under completely different pathways from the M to I phase, compared to the transition of I $\rightarrow$ M (Fig. 4B). We can clearly observe Q^{M}_{0-2Mb} decreases to an appreciable value that is even lower than the value in the final I phase. Such over-expansion can also be observed at non-local contacts (Fig. 4E), as well as by the pathway projections onto the contact probability (Fig. 4H). Combining with the results from global structural order parameters (Fig. 3), we exhibit that the over-expansion chromosome conformation in transition of M $\rightarrow$ I occur universally throughout the genomic sequence.

The irreversibility of the cell-cycle dynamics on chromosome transformation is distinctly observed by inspecting the average pathways for the two directional transitions (Fig. 4C, 4F and 4I). The local contact formation undergoes two completely separated, non-overlapped pathways for the two transitions that constitute the cell cycle. When the genomic distance range of the pairwise contact increases to non-local, the pathways tend to coincide, in particular at the stage close to the M phase (Fig. 4F and Fig. S16). It is possibly due to the highly condensed mitotic conformations that geometrically limit the number of available configurational space to explore. It is worth noting that TADs forms within $\sim$ 2Mb range (Fig. S1), so we claim that the formation and deformation of TADs during the cell cycle undergo irreversible pathways.

3.3 Heterogeneity in TAD conformational transition during the cell cycle

It is tempting to see how TADs, as structural units in chromosome [14], evolve during the cell-cycle dynamics. We have identified 40 TADs on the chromosome we investigated, spanning from 0.9 Mb to 3.4 Mb in genomic length (Fig. S1). Then we calculated the R_g of every TAD for all the trajectories and monitor the average pathways during the transitions. In transition of I $\rightarrow$ M, most of TADs proceed to the condensation, though there are already abundant contacts formed within TADs [11]. There are roughly two classes of R_g evolutions, one decreases R_g monotonically to the M phase and the other one increases R_g followed by decreasing R_g (Fig. 5A). The observation of the later one is interesting, and can be regarded as a reminiscence of recent single cell cycle Hi-C data, which clearly show that some TADs may undergo de-condensation from early G_1 to S phase before the completion of the I phase [7]. Two typical TADs are chosen to represent these two evolutions. For both of the TADs, note that the variance of the pathways are large, indicating that even one single TAD is capable to undergo highly heterogeneous pathways to accomplish the transition.

On the other hand, in transition from the M to I phase, almost all TADs have to undergo a de-condensation prior to a final condensation, though the magnitude of increasing R_g is different. The initial de-condensation may be attributed to the over-expansion process which has been observed in Fig. 3 and 4. The de-condensation processes for all TADs reach the peaks at around 2τ. These facts imply that the TADs conformational dynamics are cooperative processes in M $\rightarrow$ I transition. Furthermore, it is interesting to see TAD5 may follow the same routes in the two directional transitions with sharing extended intermediates, while TAD36 conformational transition pathway is likely irreversible. The average pathway show the last compaction processes in both transitions take place at similar time step after 1τ, implying that the kinetic rates in TADs are similar in the two directional transitions.

One of the prominent appearance of the M phase is the loss of TAD signals from missing of the TAD boundary due to the high condensation [45]. The strength of TAD can be measured by the insulation at TAD boundary [49], defined through the degree of contact depletion crossing the TAD borders [7]. It can be tracked here by monitoring the spatial distance d_{com} between the two neighboring TADs during the transitions (Fig. 5C and 5D). When a short (long) distance d_{com} is observed, the TAD insulation is weak (strong), corresponding to a loss (formation) of TAD boundary. Although there are still highly heterogeneous pathways for one single inter-TAD distance evolu-

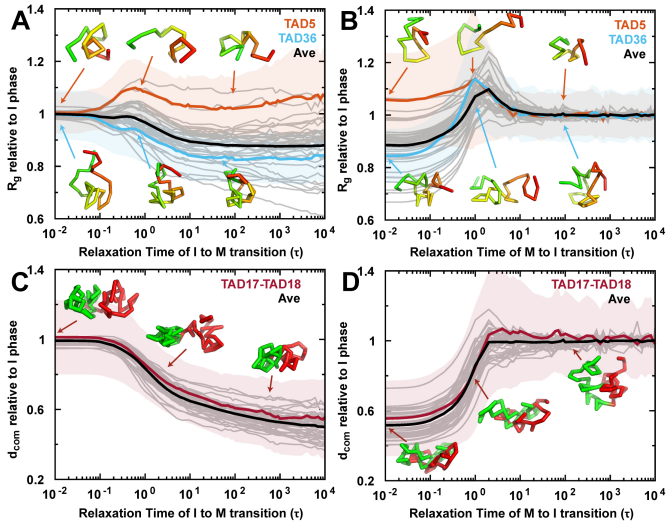

Fig. 5: TADs conformational dynamics during the cell cycle. The pathways of radius of gyration R_g for the transitions of (A) I $\rightarrow$ M and (B) M $\rightarrow$I. The relative R_g to the average values of that in the I phase for all the 40 TADs are shown in grey lines. The TAD5 (5th TAD, orange, same notation used thereafter) and TAD36 (blue) are selected for illustrations and the shadow regions are the variances. Structures of the selected TADs are shown and colored from red to green varied by genomic distance. The pathways of distance of center of mass (d_{com}) between neighboring TADs for the transitions of (A) I $\rightarrow$ M and (B) M $\rightarrow$I. The d_{com} of TAD17-TAD18 is selected for illustration and the corresponding shadow regions are the variances. Representative structures of TAD17 and TAD18 are colored red and green, respectively.

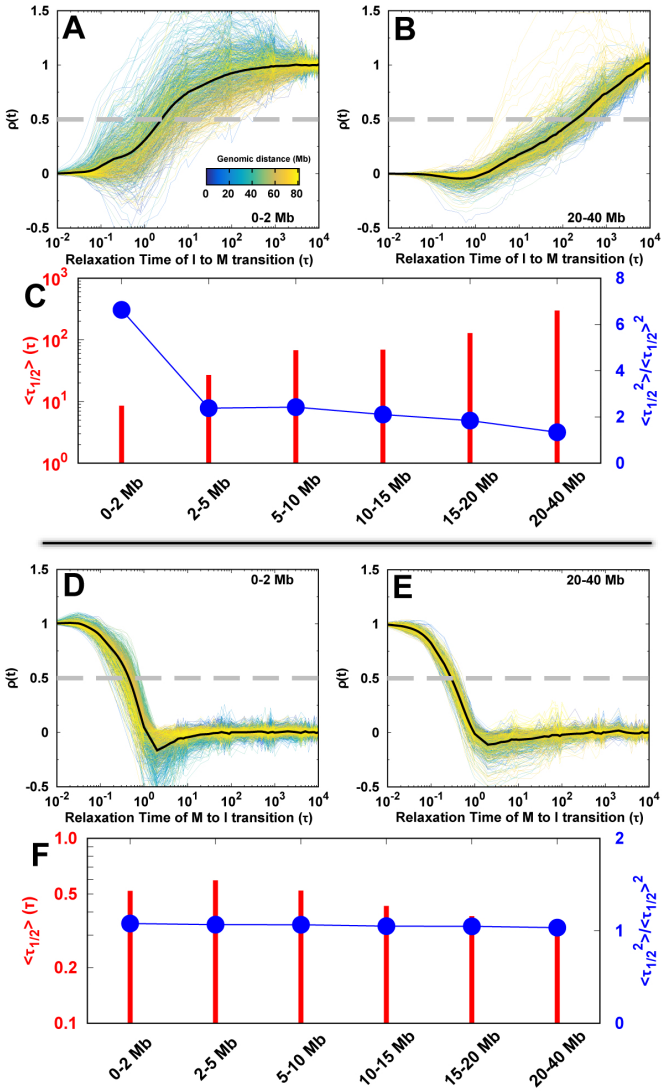

Fig. 6: Kinetics of chromosome conformational transition during the cell cycle. The degree of contact formation is calculated by $\rho(t) = (P(t) - P^I)/(P^M - P^I)$. The transition pathways for all the individual loci are shown. (A) and (B) are for $\rho(t)$ of short and long-distance contacts in I $\rightarrow$ M transition, respectively. (D) and (E) are the same with (A) and (B) but for M $\rightarrow$ I transition. The grey dashed lines in (A, B) and (D, E) dictate the position where $\rho(t)$ is half formed with associated time defined as the half life time $t_{1/2}$. (C) $t_{1/2}$ for contacts forming at different distances during the transition from the I to M phase as well as its second order moments. (F) Same with (C) but for the transition from the M to I phase.

tions, the spatial distances of the average pathways all monotonically decrease to the M phase in I $\rightarrow$ M transition. On the other hand, the over-expansion effect in transition from the M to I phase appears to be minor and most of the spatial distances of the pathways increase monotonically till reaching a plateau. Therefore, inter-TAD distance evolves more cooperatively than intra-TAD does and can possibly share the same routes in the two directional transitions.

We monitored contact probability formation evolution of each individual locus interacting with others at different genomic distances and calculated the half lift time during the two directional transitions in the cell cycle (Fig. 6). In I $\rightarrow$ M transition, the highly heterogeneous evolution at short-distance contact formation is present with the extent of heterogeneity of the pathways weakening as the genomic distance increases (Fig. 6A, 6B and Fig. S19A). There is a positive monotonic relation between the mean $\tau_{1/2}$ and genomic distance (Fig. 6C). In particular, the local (0-2 Mb) conformation forms much faster than the other non-local one does. However, by carefully examining the second order movements of $\tau_{1/2}$, we observed a very big fluctuation of $\tau_{1/2}$ at the local genomic distance of 0-2 Mb. It strongly indicates that the conformational kinetics for each individual locus is a non-Poisson process and the quantity $\tau_{1/2}$ can not be self-averaging [50], as the distribution possesses a long tail far away from the mean value (Fig. S19B). Since the formation of TADs falls in the genomic distance of $\sim$ 2 Mb, we conclude that TAD conformational dynamics in I $\rightarrow$ M transition is highly heterogeneous for each individual locus and could possibly be accomplished quite late even though the average transformation pathways are shown to be efficiently fast. When the genomic distance increases from 0-2 Mb to 2-5 Mb, $< \tau_{1/2}^2 > / < \tau_{1/2} >^2$ decreases sharply near to 2, and keeps slightly decreasing to the longer genomic distances. It indicates that at longer genomic distance beyond TAD range, chromosome transformation is highly cooperative among each individual locus and proceeds more slowly than it at TADs.

On the other hand, there appears to be little differences for the conformational evolution of individual locus at various ge-

nomic distances during the transition from the M to I phase (Fig. 6D-F and Fig. S18C). For different contacting distances, the mean $\tau_{1/2}$ show very similar small values and the second order movements of $\tau_{1/2}$ are relatively low close to 1, resulting in similar $\tau_{1/2}$ distributions (Fig. S19D). These observations all lead to a conclusion that individual chromosomal locus acts cooperatively to accomplish the transformation from the M to I phase and the kinetics is much faster than the one in the transition from the I to M phase, confirming again the irreversibility of the cell-cycle dynamics.

3.4 Broadly distributed and distinguishable bimodal structural transition state ensembles

Precisely characterizing the transition state ensemble (TSE) has always been a challenge in molecular dynamics (MD) simulations, it is anticipatively even more difficult for energy landscape-switching simulations, which corresponds to a non-adiabatic dynamics. Nevertheless, it can be approximately done by using structural reaction coordinates and assuming a structurally formed TS is located at the intermediate half way of the transition [51]. This resembles the widely used kinetic TS definition in conventional MD, where TS has the equal probability to reach reactants and products [52]. Although such definition of structural TS is not exact, it provides an informative way to extract the critical structures during the transition. Practically, we assume structural TS locates at the place when d_{rms} to the I and M phase are the same [51], where d_{rms} is the pairwise distance root-mean-square deviation.

There are two structural TSEs respectively for the two directional transitions in the cell-cycle dynamics. Overall, both of the two TSEs show broad distributions, but they are distinctly different from the structural aspects (Fig. 7). These findings are in contrast with the equilibrium process, where TSs should be the same for the forward and backward reactions if the same condition is applied. Both of the TSEs have a slight decrease in extension along PA1 relative to that in the I phase, but differentiate along PA3 (Fig. 7A). The extensions of the most probable TS structures in M $\rightarrow$ I transition resembles close to that in the I phase, while in the transition of I $\rightarrow$ M, TSEs are only structurally shortened at PA3 direction. The globally structural order parameter R_g is coincidently similar for the two TSEs with quite narrow distributions, while Δ of TSEs shows a much broader distribution and a higher cylindrical-like value in I $\rightarrow$ M than M $\rightarrow$ I transitions (Fig. 7B). The findings above all indicate that chromosomes in the two structural TSEs are condensed at similar compaction extents, but with quite different aspheric shapes.

From contact perspective, the formation of short-distance interaction is more close to the final destined M phase in the structural TSEs of I $\rightarrow$ M transition, though an over-stabilized effect can be observed at Q^M_{0-2Mb}, while the short-distance contacts of TSEs in M $\rightarrow$ I transition are fully distorted from the M phase and proceed nearly at the half way to the I phase conformation (Fig. 7C). On the other hand, the long-distance contacts in both TSEs resemble the formation in the I phase and are similarly located at the half way to the M phase conformation (Fig. 7D). We therefore deduce that the structural TSEs of the two directional transitions are largely different at the interactions within local TAD-length range and gradually become similar as the interaction distance increases (Fig. S20 and S21).

There are also apparent differences for the two directional transitions in terms of kinetic transition time (Fig. 7E). The transition from the I to M phase shows that the first passage time to structural TSEs (t_{TS}) has an extremely broad distribution along with a higher most probable value than the one in M $\rightarrow$ I transition. We attribute the difference to the formation of short-distance contacts, as they contribute to the major structural differences for the two structural TSEs.

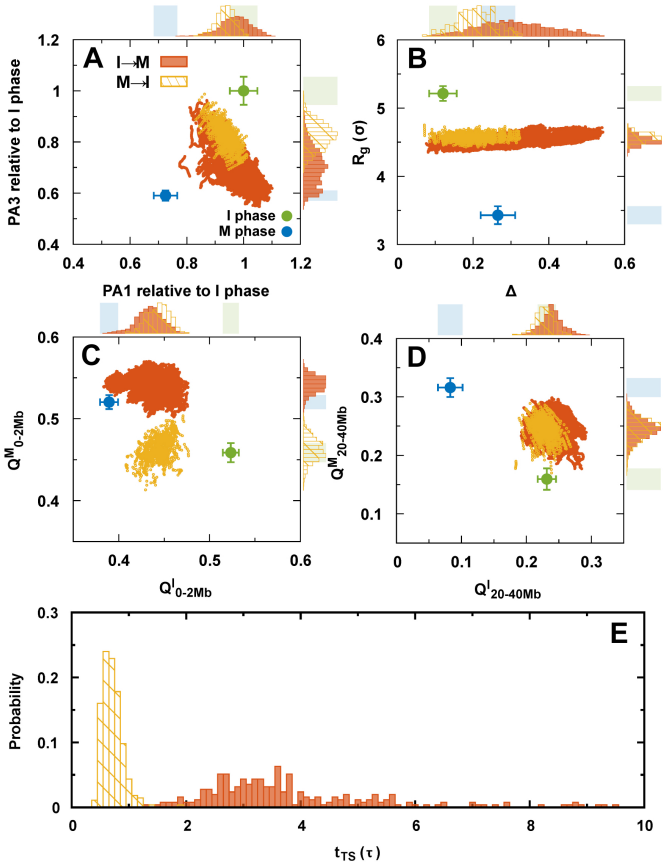

Fig. 7: Structural TSEs. (A-D) Chromosome at TSEs are described by different order parameters. There are two TSEs for transitions of I $\rightarrow$ M and M $\rightarrow$ I colored in orange and yellow respectively. The plots with points in each panel accumulate all TSs in the trajectories. The top and right side bars are probability distributions projected to different order parameters at one dimension with shadow regions indicating the values at the I (green) and M (blue) phase. (E) The distributions of the first passage times to the TSEs.

4 Discussions

We utilized a landscape-switching model to approximately take into account the non-equilibrium effects of enzymatic activities in regulating the cyclic chromosome transformation during the cell cycle. We showed that chromosome condensation deviates significantly from the reversal of decondensation. Further structural analysis on the pathways uncovered that the major deviation originates from the stage near

to the I phase and the local distance contact formation, particularly within the TAD ranges. It is worth noting that during I $\rightarrow$ M transition, this distance is similar to that of consecutive loops induced by extensive condensin II in chromosome compaction at prophase [53]. In transition of M $\rightarrow$ I, we showed that chromosome at the late stage acquires the I phase organization via a slight mandatory condensation at both the short and long-distance ranges. It is reminiscent of chromosome interphase compaction, which is modulated by an intimate collaboration of cohesion [54, 55] and Condensin II [56, 57]. These SMC proteins are specifically oriented to be effective at various distances including the establishment of TADs, and large-scale spatial partitioning of compartments and inter-chromosome territory. We therefore assume that the irreversibility in chromosome transformation during the cell-cycle dynamics is biologically attributed to the different enzymatic activities participating in the deformation (formation) of the I phase chromosome during mitotic (exit) process [44, 37]. Our statements can be potentially assessed via targeted Hi-C experiments. In this respect, a multiplexed Hi-C with advanced cell cycle phasing particularly focused on the mitotic exit process would provide a comprehensive chromosome decondensation description. This will make essential physical and quantitative complementarity to the available experimental descriptions on chromosome condensation [45, 7].

The results of our model draw a quite complete picture of chromosome transformation during the cell-cycle dynamics. The transition pathways observed in our simulations are highly heterogeneous, implying the dynamics is stochastic. But they are far from the random, following evident routes. This reflects the cell-to-cell variability discovered in recent single-cell cell cycle Hi-C data [58, 7]. Our description on chromosome condensation is in good agreement with the two-stage mitotic chromosome folding hypothesis [45]. The active anisotropic chromosome compaction from the I to M phase is likely an outcome of asynchronous contact formations at various distances, where the local domains form much faster than the non-local contacts. In accompany with the loop extrusion models and other previous experimental findings [45, 9], we can reasonably make assumptions on the mechanism of mitotic chromosome morphogenesis. The initial formation of short-distance contacts establishes the chromosomal scaffold axes with the loosely organized loops mainly contributed by condensin II [9]. Later on, the long-range contacts shape the chromosome into a condensed cylinder. At late stage some proportions of local contact stabilization (Fig. S19B) likely correspond to the formation of smaller nested loops by condensin I at prometaphase [9]. On the contrary, M $\rightarrow$ I transition isotropically expands at the early stage quickly. It implies an efficient mitotic exit with releasing the condensins that are previously involved during the condensation process. The observed over-expanded chromosome configurations during mitotic exit process can topologically increase the accessible surface to the proteins in the bulk, thus are biologically beneficial. Such effect can be particularly important along with the facts that interphase chromosome experiences a confinement-induced glassy dynamics in crowded cellular environment [35]. Further assessments on our hypothesis are in demand. Finally, it is interesting to see that the chromosome mitotic folding mechanism is reminiscent of protein folding framework model, where the local contacts fold prior to non-local ones, while the concurrent local and non-local structural formation of chromosome during mitotic exit process resembles the nucleation-condensation mechanism of protein folding [59]. Therefore, chromosome condensation and de-condensation mechanisms are the reflections of the underlying local and non-local interaction interplay during the cell cycle process.

Our investigations on the cyclic structural changes of intra- and inter-TAD provided detailed descriptions of TAD condensation [11] and insulation [49] during the cell cycle. In line with the recent single-cell Hi-C experiments [7], the decondensed TADs were largely observed at the I phase, signifying an open chromatin that are functionally advantageous to gene regulation [13]. Additionally, experiments observed that some TADs may de-condense though the overall trend of TAD condensation shows monotonic strengthening. In our simulations, we observed such deviation on particular TADs, and confirmed the heterogeneity in TADs transformation. On the other hand, the insulation of TAD evolves more cooperatively than TAD (de)condensation does, stating that the spatial proximity of neighboring TADs can serve as an indicator of cell cycle progression [7].

It is tempting to match our kinetic simulations to the real cell-cycle dynamics based on the current available experimental facts. Bearing in mind, our simulation starts from mid-G_1 in the I phase. We can attribute the initial decrease of TAD insulation at $\sim 0.1 - 1\tau$ (Fig. 5C) to be the arrival of the S or G_2 in the I phase, based on the experimental findings [7]. Then by using $\tau_{1/2}$ at quasi-short-distance contact range of 2-5Mb as an indicator of loss of TAD boundary, we can deduce the time of prophase is $\sim 20\tau$. It is coincidentally to find that the time when the slope of the average pathways on PA extension transition reaches the intermediate half values is also roughly $\sim 20\tau$ (Fig. 3A). Such point of time can be used to separate the first stage of condensin II-dependent linear looping in prophase [60] and second stage of axial compression in prometaphase [61]. Further relaxation of chromosome from prometaphase to metaphase in our simulations can take up to 1000τ and more, which is seemingly consistent with the experimental findings of a long duration time in prometaphase [45]. Overall, our simulations have well predicted the key progression phases associated with the correct chromosome morphogenesis during the cell cycle. There are two factors worth noting here. (1) The underlying kinetics of the system is based on landscape-switching. The timescale estimated in simulations may not be directly used to infer the real reaction rates. (2) We could not observe additional axial compression of chromosome in anaphase after metaphase [62]. The prediction of anaphase is beyond our simulation scope, as we have approximately assumed metaphase chromosome to be the final destined condensed states in our models.

The simulation strategy applied here is based on the energy landscape theory, which has been widely used to understand the folding and function of proteins [63]. The extension of energy landscape to genomic dynamics seems sensible, however attentions should be paid during the application [64]. Beyond the thermodynamic distributions, here our studies and other previous studies showed that the effective energy landscapes are also capable of characterizing the correct kinetics on chromosome anomalous diffusion [47, 65]. These features suggest

a broad applicability of the energy landscape approach into much bigger and more complex system, e. g. chromosome organization, beyond proteins. Nevertheless, the question still remains. Is the effective energy landscape sufficient to describe the chromosome transformation during the cell cycle? Direct utilization of energy landscape concept here seems to be inappropriate, as the driving forces of the cell cycle originate mainly from the non-equilibrium chemical reactions. However, the transition process can be approximately referred to as a switch between the two phases, where the prior and posterior energy landscape for each phase are still effective and corrective for chromosome dynamics. The assessments on the energy landscape-switching model have been done by comparing the mitotic chromosome folding within experiments and our simulations. The emergent pictures are highly consistent with the experiments, supporting the validity and success of our model. The irreversibility of the pathways uncovered in our simulations is an outcome of non-equilibrium dynamics [66], and would be absent if an equilibrium investigation approach is applied. Therefore, our work serves as an appealing manifestation that energy landscape with rationally incorporating the non-equilibrium effect works effectively on genomic level.

In summary, we developed an energy landscape-switching model to probe the chromosome structural transformation during the cell cycle. The predictions are compared to current available experiments and well reproduced the mitotic chromosome folding mechanism that was previously proposed. The irreversibility revealed by us in the cell cycle can be tested by the further experimental investigations. Our theoretical results can guide future experiments to address the roles of SMC protein complexes and other key molecular components that are found to widely participate into the mitosis. Our findings can ultimately aid to the profound understanding of chromosome functional reorganization in cell developments and pathological disorganization in cancer cells.

5 Materials and Methods

5.1 Hi-C data processing

The Hi-C data of interphase and metaphase for HeLa cells were downloaded from ArrayExpress database with accession number E-MTAB-1948 [45]. It has been established that the Hi-C data of different sub-stages within interphase display quite similar patterns at both short- and long-range pairwise contact regions and are highly correlated [45], we therefore used mid-G_1 Hi-C data to approximately represent the entire interphase (I phase). On the other hand, we use metaphase Hi-C data to represent the mitotic phase (M phase). Two replicas of the Hi-C data from each phase were combined together and the analysis process was proceeded routinely by the HiC-Pro software [67]. To normalize the pairwise contact frequencies into contact probabilities, which are more straightforward to be implemented into the following polymer simulations, we applied the same method proposed in [28] by reasonably assuming the neighboring beads are always in contact with a probability of $P_{i,i\pm1} \equiv 1.0$. All the Hi-C matrices are done at 100-kb resolution. This is high enough to monitor the chromosome dynamics. We then focused on a long segment on chromosome 5 from 80 Mb to 161.1 Mb, which eventually leads to 812 beads in the system for the following polymer simulations.

5.2 Chromosome simulations guided by maximum entropy principle

The I and M phase chromosome structures are produced by a maximum entropy principle approach with practically incorporating the experimental Hi-C data into the generic polymer simulations [28, 29]. The prominent outcome of the maximum entropy principle approach is to generate an ensemble of chromosome structures that can collectively reconstruct the experimental Hi-C, and furthermore remain as close as possible to the prior distribution from the generic polymer simulations by means of maximizing the relative entropy [68]. More importantly here, the maximum entropy principle can give rise to an interaction potential energy function (i.e. force field) for simulations that are rationally restrained by the experimental ensemble-average Hi-C data, and this eventually leads to a minimally biased energy landscape [28]. Such effective energy landscape not only can have an accurate description of chromosome thermodynamic distributions that constrain the Hi-C data-based contact probability, but also can ultimately provide the details of the kinetics within and between each metastable state during the simulations (Fig. S5).

5.3 Cell-cycle dynamics revealed by energy landscape-switching model

We developed an energy landscape-switching model to simulate the chromosome transformation during the cell cycle. This goes beyond the previous studies for allosteric protein dynamics [69, 51]. The cell cycle process has been simplified to be made up by two transitions including from the I to M phase and the M to I phase. The algorithm is implemented in the following three steps. Firstly, chromosome in the I phase (M phase) is simulated by the corresponding potential energy function (landscape) obtained from the maximum entropy principle simulation for a duration of $5 \times 10^3 \tau$, where τ is the simulation time unit, approximate to $2s$ in real time (Fig. S5). Then, a sudden switch of the energy landscape from the I phase (M phase) to the M phase (I phase) is performed. Finally, the simulations under the new energy landscape of the M phase (I phase) run for $1 \times 10^4 \tau$. In practice, simulations are initialized from the structures obtained after clustering the trajectories of the maximum entropy principle for the I or M phase and only the clusters with populations higher than 1% are selected (Fig. S4 and S8). This finally leads to 52 and 56 clusters for the I and M phase chromosome ensemble, respectively. For each cluster, five structures the most close to the cluster centre are chosen. Therefore, we accumulated 260 transitions from the I to M phase, as well as 280 transitions from the M to I phase.

References

[1] Giacomo Cavalli and Tom Misteli. Functional implications of genome topology. *Nature structural & molecular biology*,

20(3):290, 2013.

[2] Christian Lanctôt, Thierry Cheutin, Marion Cremer, Giacomo Cavalli, and Thomas Cremer. Dynamic genome architecture in the nuclear space: regulation of gene expression in three dimensions. *Nature Reviews Genetics*, 8(2):104, 2007.

[3] Job Dekker, Karsten Rippe, Martijn Dekker, and Nancy Kleckner. Capturing chromosome conformation. *science*, 295(5558):1306–1311, 2002.

[4] Erez Lieberman-Aiden, Nynke L Van Berkum, Louise Williams, Maxim Imakaev, Tobias Ragoczy, Agnes Telling, Ido Amit, Bryan R Lajoie, Peter J Sabo, Michael O Dorschner, et al. Comprehensive mapping of long-range interactions reveals folding principles of the human genome. *Science*, 326(5950):289–293, 2009.

[5] Yasutaka Kakui, Adam Rabinowitz, David J Barry, and Frank Uhlmann. Condensin-mediated remodeling of the mitotic chromatin landscape in fission yeast. *Nature genetics*, 49(10):1553, 2017.

[6] Luciana Lazar-Stefanita, Vittore F Scolari, Guillaume Mercy, Héloïse Muller, Thomas M Guérin, Agnès Thierry, Julien Mozziconacci, and Romain Koszul. Cohesins and condensins orchestrate the 4d dynamics of yeast chromosomes during the cell cycle. *The EMBO journal*, 36(18):2684–2697, 2017.

[7] Takashi Nagano, Yaniv Lubling, Csilla Várnai, Carmel Dudley, Wing Leung, Yael Baran, Netta Mendelson Cohen, Steven Wingett, Peter Fraser, and Amos Tanay. Cell-cycle dynamics of chromosomal organization at single-cell resolution. *Nature*, 547(7661):61, 2017.

[8] Stephanie Andrea Schalbetter, Anton Goloborodko, Geoffrey Fudenberg, Jon-Matthew Belton, Catrina Miles, Miao Yu, Job Dekker, Leonid Mirny, and Jonathan Baxter. Smc complexes differentially compact mitotic chromosomes according to genomic context. *Nature cell biology*, 19(9):1071, 2017.

[9] Johan H Gibcus, Kumiko Samejima, Anton Goloborodko, Itaru Samejima, Natalia Naumova, Johannes Nuebler, Masato T Kanemaki, Linfeng Xie, James R Paulson, William C Earnshaw, et al. A pathway for mitotic chromosome formation. *Science*, 359(6376):eaao6135, 2018.

[10] Jesse R Dixon, Siddarth Selvaraj, Feng Yue, Audrey Kim, Yan Li, Yin Shen, Ming Hu, Jun S Liu, and Bing Ren. Topological domains in mammalian genomes identified by analysis of chromatin interactions. *Nature*, 485(7398):376, 2012.

[11] Tom Sexton, Eitan Yaffe, Ephraim Kenigsberg, Frédéric Bantignies, Benjamin Leblanc, Michael Hoichman, Hugues Parrinello, Amos Tanay, and Giacomo Cavalli. Three-dimensional folding and functional organization principles of the drosophila genome. *Cell*, 148(3):458–472, 2012.

[12] Chunhui Hou, Li Li, Zhaohui S Qin, and Victor G Corces. Gene density, transcription, and insulators contribute to the partition of the drosophila genome into physical domains. *Molecular cell*, 48(3):471–484, 2012.

[13] Elphège P Nora, Bryan R Lajoie, Edda G Schulz, Luca Giorgetti, Ikuhiro Okamoto, Nicolas Servant, Tristan Piolot, Nynke L van Berkum, Johannes Meisig, John Sedat, et al. Spatial partitioning of the regulatory landscape of the x-inactivation centre. *Nature*, 485(7398):381, 2012.

[14] Jesse R Dixon, David U Gorkin, and Bing Ren. Chromatin domains: the unit of chromosome organization. *Molecular cell*, 62(5):668–680, 2016.

[15] Job Dekker. Two ways to fold the genome during the cell cycle: insights obtained with chromosome conformation capture. *Epigenetics & chromatin*, 7(1):25, 2014.

[16] Benjamin D Pope, Tyrone Ryba, Vishnu Dileep, Feng Yue, Weisheng Wu, Olgert Denas, Daniel L Vera, Yanli Wang, R Scott Hansen, Theresa K Canfield, et al. Topologically associating domains are stable units of replication-timing regulation. *Nature*, 515(7527):402, 2014.

[17] David U Gorkin, Danny Leung, and Bing Ren. The 3d genome in transcriptional regulation and pluripotency. *Cell stem cell*, 14(6):762–775, 2014.

[18] Leonid A Mirny. The fractal globule as a model of chromatin architecture in the cell. *Chromosome research*, 19(1):37–51, 2011.

[19] Joel M Gottesfeld and Douglass J Forbes. Mitotic repression of the transcriptional machinery. *Trends in biochemical sciences*, 22(6):197–202, 1997.

[20] Kazuhiro Maeshima, Satoru Ide, Kayo Hibino, and Masaki Sasai. Liquid-like behavior of chromatin. *Current opinion in genetics & development*, 37:36–45, 2016.

[21] Masaki Sasai and Peter G Wolynes. Stochastic gene expression as a many-body problem. *Proceedings of the National Academy of Sciences*, 100(5):2374–2379, 2003.

[22] Bin Zhang and Peter G Wolynes. Stem cell differentiation as a many-body problem. *Proceedings of the National Academy of Sciences*, 111(28):10185–10190, 2014.

[23] Alexandra Zidovska, David A Weitz, and Timothy J Mitchison. Micron-scale coherence in interphase chromatin dynamics. *Proceedings of the National Academy of Sciences*, 110(39):15555–15560, 2013.

[24] Luis Aragon, Enrique Martinez-Perez, and Matthias Merkenschlager. Condensin, cohesin and the control of chromatin states. *Current opinion in genetics & development*, 23(2):204–211, 2013.

[25] Frank Uhlmann. Smc complexes: from dna to chromosomes. *Nature reviews Molecular cell biology*, 17(7):399, 2016.

[26] Shenshen Wang and Peter G Wolynes. Communication: Effective temperature and glassy dynamics of active matter. *Journal of Chemical Physics*, 135(5):051101–051101, 2011.

[27] S Wang and PG Wolynes. Tensegrity and motor-driven effective interactions in a model cytoskeleton. *The Journal of chemical physics*, 136(14):145102, 2012.

[28] Bin Zhang and Peter G Wolynes. Topology, structures, and energy landscapes of human chromosomes. *Proceedings of the National Academy of Sciences*, 112(19):6062–6067, 2015.

[29] Bin Zhang and Peter G Wolynes. Shape transitions and chiral symmetry breaking in the energy landscape of the mitotic chromosome. *Physical review letters*, 116(24):248101, 2016.

[30] Qiang Lu and Jin Wang. Single molecule conformational dynamics of adenylate kinase: energy landscape, structural correlations, and transition state ensembles. *Journal of the American Chemical Society*, 130(14):4772–4783, 2008.

[31] Yong Wang, Linfeng Gan, Erkang Wang, and Jin Wang. Exploring the dynamic functional landscape of adenylate kinase modulated by substrates. *Journal of chemical theory and computation*, 9(1):84–95, 2012.

[32] Xiakun Chu, Fei Liu, Brian A Maxwell, Yong Wang, Zucai Suo, Haijun Wang, Wei Han, and Jin Wang. Dynamic conformational change regulates the protein-dna recognition: an investigation on binding of a y-family polymerase to its target dna. *PLoS computational biology*, 10(9):e1003804, 2014.

[33] Kei-ichi Okazaki, Nobuyasu Koga, Shoji Takada, Jose N Onuchic, and Peter G Wolynes. Multiple-basin energy landscapes for large-amplitude conformational motions of proteins:

Structure-based molecular dynamics simulations. *Proceedings of the National Academy of Sciences*, 103(32):11844–11849, 2006.

[34] Paul C Whitford, Osamu Miyashita, Yaakov Levy, and José N Onuchic. Conformational transitions of adenylate kinase: switching by cracking. *Journal of molecular biology*, 366(5):1661–1671, 2007.

[35] Hongsuk Kang, Young-Gui Yoon, D Thirumalai, and Changbong Hyeon. Confinement-induced glassy dynamics in a model for chromosome organization. *Physical review letters*, 115(19):198102, 2015.

[36] Jin Wang. Landscape and flux theory of non-equilibrium dynamical systems with application to biology. *Advances in Physics*, 64(1):1–137, 2015.

[37] Wolfram Antonin and Heinz Neumann. Chromosome condensation and decondensation during mitosis. *Current opinion in cell biology*, 40:15–22, 2016.

[38] Jin Wang, Chunhe Li, and Erkang Wang. Potential and flux landscapes quantify the stability and robustness of budding yeast cell cycle network. *Proceedings of the National Academy of Sciences*, 107(18):8195–8200, 2010.

[39] Chunhe Li and Jin Wang. Landscape and flux reveal a new global view and physical quantification of mammalian cell cycle. *Proceedings of the National Academy of Sciences*, 111(39):14130–14135, 2014.

[40] Jin Wang, Li Xu, and Erkang Wang. Potential landscape and flux framework of nonequilibrium networks: Robustness, dissipation, and coherence of biochemical oscillations. *Proceedings of the National Academy of Sciences*, 105(34):12271–12276, 2008.

[41] Umberto Galderisi, Francesco Paolo Jori, and Antonio Giordano. Cell cycle regulation and neural differentiation. *Oncogene*, 22(33):5208, 2003.

[42] Angelo Rosa and Ralf Everaers. Structure and dynamics of interphase chromosomes. *PLoS computational biology*, 4(8):e1000153, 2008.

[43] Guido Tiana, Assaf Amitai, Tim Pollex, Tristan Piolot, David Holcman, Edith Heard, and Luca Giorgetti. Structural fluctuations of the chromatin fiber within topologically associating domains. *Biophysical journal*, 110(6):1234–1245, 2016.

[44] Neville Cobbe, Ellada Savvidou, and Margarete MS Heck. Diverse mitotic and interphase functions of condensins in drosophila. *Genetics*, 172(2):991–1008, 2006.

[45] Natalia Naumova, Maxim Imakaev, Geoffrey Fudenberg, Ye Zhan, Bryan R Lajoie, Leonid A Mirny, and Job Dekker. Organization of the mitotic chromosome. *Science*, 342(6161):948–953, 2013.

[46] Soya Shinkai, Tadasu Nozaki, Kazuhiro Maeshima, and Yuichi Togashi. Dynamic nucleosome movement provides structural information of topological chromatin domains in living human cells. *PLoS computational biology*, 12(10):e1005136, 2016.

[47] Lei Liu, Guang Shi, D Thirumalai, and Changbong Hyeon. Chain organization of human interphase chromosome determines the spatiotemporal dynamics of chromatin loci. *PLoS computational biology*, 14(12):e1006617, 2018.

[48] Ruxandra I Dima and D Thirumalai. Asymmetry in the shapes of folded and denatured states of proteins. *The Journal of Physical Chemistry B*, 108(21):6564–6570, 2004.

[49] Emily Crane, Qian Bian, Rachel Patton McCord, Bryan R Lajoie, Bayly S Wheeler, Edward J Ralston, Satoru Uzawa, Job Dekker, and Barbara J Meyer. Condensin-driven remodelling of x chromosome topology during dosage compensation. *Nature*, 523(7559):240, 2015.

[50] Xiakun Chu, Linfeng Gan, Erkang Wang, and Jin Wang. Quantifying the topography of the intrinsic energy landscape of flexible biomolecular recognition. *Proceedings of the National Academy of Sciences*, 110(26):E2342–E2351, 2013.

[51] Changbong Hyeon, George H Lorimer, and D Thirumalai. Dynamics of allosteric transitions in groel. *Proceedings of the National Academy of Sciences*, 103(50):18939–18944, 2006.

[52] Rose Du, Vijay S Pande, Alexander Yu Grosberg, Toyoichi Tanaka, and Eugene S Shakhnovich. On the transition coordinate for protein folding. *The Journal of chemical physics*, 108(1):334–350, 1998.

[53] Takao Ono, Ana Losada, Michiko Hirano, Michael P Myers, Andrew F Neuwald, and Tatsuya Hirano. Differential contributions of condensin i and condensin ii to mitotic chromosome architecture in vertebrate cells. *Cell*, 115(1):109–121, 2003.

[54] Suhas SP Rao, Su-Chen Huang, Brian Glenn St Hilaire, Jesse M Engreitz, Elizabeth M Perez, Kyong-Rim Kieffer-Kwon, Adrian L Sanborn, Sarah E Johnstone, Gavin D Bascom, Ivan D Bochkov, et al. Cohesin loss eliminates all loop domains. *Cell*, 171(2):305–320, 2017.

[55] Wibke Schwarzer, Nezar Abdennur, Anton Goloborodko, Aleksandra Pekowska, Geoffrey Fudenberg, Yann Loe-Mie, Nuno A Fonseca, Wolfgang Huber, Christian H Haering, Leonid Mirny, et al. Two independent modes of chromatin organization revealed by cohesin removal. *Nature*, 551(7678):51, 2017.

[56] Osamu Iwasaki, Christopher J Corcoran, and Ken-ichi Noma. Involvement of condensin-directed gene associations in the organization and regulation of chromosome territories during the cell cycle. *Nucleic acids research*, 44(8):3618–3628, 2015.

[57] Leah F Rosin, Son C Nguyen, and Eric F Joyce. Condensin ii drives large-scale folding and spatial partitioning of interphase chromosomes in drosophila nuclei. *PLoS genetics*, 14(7):e1007393, 2018.

[58] Takashi Nagano, Yaniv Lubling, Tim J Stevens, Stefan Schoenfelder, Eitan Yaffe, Wendy Dean, Ernest D Laue, Amos Tanay, and Peter Fraser. Single-cell hi-c reveals cell-to-cell variability in chromosome structure. *Nature*, 502(7469):59, 2013.

[59] Stefano Gianni, Nicholas R Guydosh, Faaizah Khan, Teresa D Caldas, Ugo Mayor, George WN White, Mari L DeMarco, Valerie Daggett, and Alan R Fersht. Unifying features in protein-folding mechanisms. *Proceedings of the National Academy of Sciences*, 100(23):13286–13291, 2003.

[60] Natashe Kireeva, Margot Lakonishok, Igor Kireev, Tatsuya Hirano, and Andrew S Belmont. Visualization of early chromosome condensation: a hierarchical folding, axial glue model of chromosome structure. *J Cell Biol*, 166(6):775–785, 2004.

[61] Paul S Maddox, Nathan Portier, Arshad Desai, and Karen Oegema. Molecular analysis of mitotic chromosome condensation using a quantitative time-resolved fluorescence microscopy assay. *Proceedings of the National Academy of Sciences*, 103(41):15097–15102, 2006.

[62] Felipe Mora-Bermúdez, Daniel Gerlich, and Jan Ellenberg. Maximal chromosome compaction occurs by axial shortening in anaphase and depends on aurora kinase. *Nature cell biology*, 9(7):822, 2007.

[63] Joseph D Bryngelson, Jose Nelson Onuchic, Nicholas D Socci, and Peter G Wolynes. Funnels, pathways, and the energy landscape of protein folding: a synthesis. *Proteins: Structure, Function, and Bioinformatics*, 21(3):167–195, 1995.

[64] Bin Zhang and Peter G Wolynes. Genomic energy landscapes. *Biophysical journal*, 112(3):427–433, 2017.

[65] Michele Di Pierro, Davit A Potoyan, Peter G Wolynes, and José N Onuchic. Anomalous diffusion, spatial coherence, and viscoelasticity from the energy landscape of human chromosomes. *Proceedings of the National Academy of Sciences*, 115(30):7753–7758, 2018.

[66] Carlos Bustamante, Jan Liphardt, and Felix Ritort. The nonequilibrium thermodynamics of small systems. *Physics Today*, 58(7):43–48, 2005.

[67] Nicolas Servant, Nelle Varoquaux, Bryan R Lajoie, Eric Viara, Chong-Jian Chen, Jean-Philippe Vert, Edith Heard, Job Dekker, and Emmanuel Barillot. Hic-pro: an optimized and flexible pipeline for hi-c data processing. *Genome biology*, 16(1):259, 2015.

[68] Andrea Cesari, Sabine Reißer, and Giovanni Bussi. Using the maximum entropy principle to combine simulations and solution experiments. *Computation*, 6(1):15, 2018.

[69] Nobuyasu Koga and Shoji Takada. Folding-based molecular simulations reveal mechanisms of the rotary motor f1–atpase. *Proceedings of the National Academy of Sciences*, 103(14):5367–5372, 2006.